29. Crone, B. *et al.* Large-scale complementary integrated circuits based on organic transistors. *Nature* **403,** 521–523 (2000).
30. Mooij, J. E. *et al.* Josephson persistent-current qubit. *Science* **285,** 1036–1039 (1999).
31. Verthamer, N. R., Helfand, E. & Hohenberg, P. C. Temperature and purity dependence of the superconducting field, Hc2, III. Electron spin and spin-orbit effects. *Phys. Rev.* **147,** 295–303 (1966).

Acknowledgements

We thank E. A. Chandross, B. Crone, H. E. Katz, H. Y. Hwang, A. J. Lovinger and T. Siegrist for discussions, and E. Bucher for the use of equipment.

Correspondence and requests for materials should be addressed to J.H.S. (e-mail: hendrik@lucent.com).

An efficient room-temperature silicon-based light-emitting diode

Wai Lek Ng*, M. A. Lourenço*, R. M. Gwilliam*, S. Ledain†, G. Shao† & K. P. Homewood*

** School of Electronic Engineering, Information Technology & Mathematics; † School of Mechanical and Materials Engineering, University of Surrey, Guildford, Surrey, GU2 7XH, UK*

There is an urgent requirement for an optical emitter that is compatible with standard, silicon-based ultra-large-scale integration (ULSI) technology[1]. Bulk silicon has an indirect energy bandgap and is therefore highly inefficient as a light source, necessitating the use of other materials for the optical emitters. However, the introduction of these materials is usually incompatible with the strict processing requirements of existing ULSI technologies. Moreover, as the length scale of the devices decreases, electrons will spend increasingly more of their time in the connections between components; this interconnectivity problem could restrict further increases in computer chip processing power and speed in as little as five years. Many efforts have therefore been directed, with varying degrees of success, to engineering silicon-based materials that are efficient light emitters[2–7]. Here, we describe the fabrication, using standard silicon processing techniques, of a silicon light-emitting diode (LED) that operates efficiently at room temperature. Boron is implanted into silicon both as a dopant to form a p–n junction, as well as a means of introducing dislocation loops. The dislocation loops introduce a local strain field, which modifies the band structure and provides spatial confinement of the charge carriers. It is this spatial confinement which allows room-temperature electroluminescence at the band-edge. This device strategy is highly compatible with ULSI technology, as boron ion implantation is already used as a standard method for the fabrication of silicon devices.

There have been great efforts over the past decade to obtain useful, that is, technologically viable and efficient, light emission from silicon both in the visible and infrared regions of the spectrum. In the visible regions, porous silicon[2] and other quantized systems, such as silicon/silicon dioxide superlattices[3] and silicon nanoprecipitates in silicon dioxide[4], have been the main emphasis. In the infrared region, systems such as erbium in silicon[5], silicon/germanium[6] and, more recently, iron disilicide[7] offer potential routes. No approach has so far been applied commercially. The reasons for this are a combination of the lack of genuine or perceived compatibility with conventional ULSI technology and, in the case of infrared emitters, high thermal quenching giving very poor room-temperature efficiencies.

Here we use a new approach—dislocation engineering, using conventional ULSI technology—that gives efficient light emission in silicon at room temperature.

Because of its indirect bandgap, silicon is fundamentally a poor emitter of light. The main reason for this is that fast non-radiative recombination routes dominate the slower radiative route in this material. Indeed, in bulk silicon, at room temperature, radiative emission is normally entirely absent. However, if recombination through the non-radiative routes can be prevented, the radiative emission could in principle be enhanced. Non-radiative recombination is the result of diffusion of carriers to point defects in the silicon where efficient non-radiative recombination then occurs. Despite the low defect concentrations in good quality silicon this non-radiative route is always completely dominant. A way of enhancing the radiative efficiency would be to prevent the carrier diffusion. If silicon can be formed as clusters then strong band-edge photoluminescence is possible[8], but thus far this has only been achieved by incorporating these clusters inside large bandgap insulating oxides. However, the insulating matrix prevents efficient carrier injection, making devices difficult to produce. Similar but much weaker (with efficiencies up to about 8×10^{-6}) band-edge emission has also been observed in laser-recrystallized silicon[9], but no explanation of its origin was presented.

We have made use of the controlled introduction of dislocation loops using conventional ion implantation and thermal processing. The dislocation loop array, if appropriately produced, introduces a strain field in three dimensions that modifies the bandgap of the

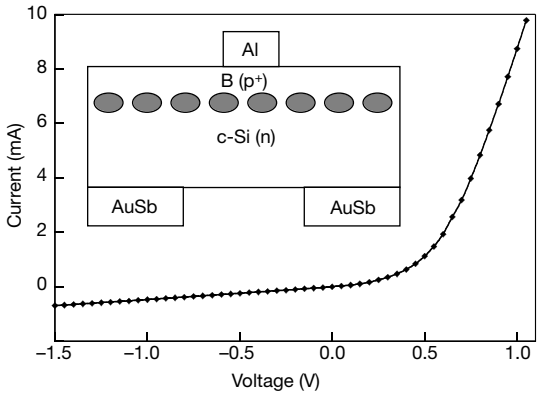

Figure 1 The current–voltage plot for the device measured at room temperature. Inset, a schematic of the light-emitting diode (LED) device. The top and bottom ohmic contacts are formed by Al and AuSb respectively. The infrared light is emitted through the window left in the bottom contact.

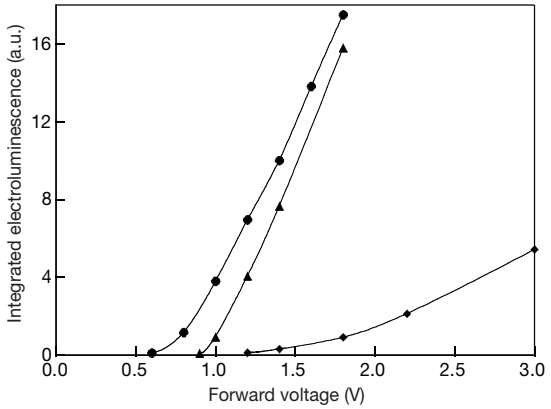

Figure 2 Plots of the integrated electroluminescence intensity as a function of applied forward voltage at various temperatures: 80 K (diamonds), 180 K (triangles) and 300 K (circles).

© 2001 Macmillan Magazines Ltd

silicon in such a way that the silicon itself can be used to provide spatial confinement in three dimensions. To minimize the number of process steps, in the device described, boron implantation has been used both to introduce the dislocation loop array and as the p-type dopant to form a p–n junction in an n-type silicon substrate. However, another implant species such as the host silicon could be used to form the dislocations so that the dislocation engineering and subsequent doping to form the p–n junction can be achieved independently. The device operates as a conventional light-emitting diode under forward bias.

A simple diagram of the device is shown in the inset to Fig. 1. The device reported here was made by implanting boron at a dose of 1×10^{15} cm^{-2} at an energy of 30 keV. The sample was subsequently annealed in a nitrogen atmosphere for 20 minutes at 1,000 °C to form the dislocation loop array and activate the boron dopants. The implants were made into a device grade CZ (Czochralski) n-type silicon substrate of resistivity 2–4 Ω cm. An important point to emphasize at this stage is that all these process steps are entirely conventional and are therefore completely compatible with ULSI technology, allowing immediate implementation on a standard fabrication line. The array of dislocation loops formed has been observed using cross-sectional transmission electron microscopy. The array is situated in a planar region parallel to, and around 100 nm from, the p–n junction. The dislocation loops are typically about 80–100 nm in diameter and are spaced around 20 nm apart. The strain field at the edge of the dislocation loop is high and falls off around each loop approximately with the inverse of distance. The magnitude and sign of the stress at the edge of the dislocation loop which determines the confining potential can be calculated using the standard elastic theory of dislocations[10] and the known values of the Poisson's ratio, 0.42, and Young's modulus, 113 GPa, for silicon. We obtain a value for the maximum stress at the outside edge (1.2 Å out) of the interstitial dislocation loop of 25–50 GPa, which will cause an increase in bandgap energy at the edge of 325–750 meV. A complete description of the stress field across the device, which is just the superposition of the stress field of all the dislocations, is complicated and will vary in detail across and between samples. However, given the inverse distance dependence of the stress around the loops, the local stress at any point is entirely dominated by the superposition of the stress field of only the closest dislocations. As carriers are injected across the junction they encounter a blocking potential that varies in height depending on the direction of their instantaneous velocity, from about 750 meV in the direction of and across a loop, down to about 20 meV at a point equidistant between two adjacent dislocations. It is this blocking potential that confines carriers close to the junction region. The varying potential falls away approximately as inverse distance back towards the junction at which point it is less than about 10 meV. Consequently, the barrier height and the onset of injection is not significantly changed. Any carriers moving back across the junction are, under steady state conditions, dynamically replaced by others moving in the forward direction.

After implantation and annealing, ohmic contacts consisting of AuSb eutectic and Al were applied to the back and front of the sample respectively. The ohmic contacts were sintered at 360 °C for 2 min. The top contact was 1 mm in diameter and, as the silicon substrate is still nearly transparent at the emission wavelength of 1,150 nm, a window was left in the larger back contact to allow the electroluminescence (EL) through. Front window devices have also been fabricated. Current–voltage (I–V) measurements were made between the back and front contacts to check that the device is behaving as a diode. An I–V plot, characteristic of the fully processed and working device, is shown in Fig. 1.

The device was mounted into a mechanical holder inside a continuous flow liquid-nitrogen cryostat. Light from the device was focused into a conventional 0.5 m spectrometer and collected by a liquid-nitrogen-cooled germanium p–i–n detector. EL measurements were then taken from 80 K to above room temperature. The onset of EL was observed as the diode turns on under forward bias. No EL is observed under reverse bias. The integrated EL intensity as a function of applied forward voltage is shown in Fig. 2 for several temperatures. The turn-on voltage at room temperature is typical of a conventional silicon diode operating under forward injection. The full EL spectra taken, as a function of temperature, at a forward current of 50 mA, are shown in Fig. 3. The low-temperature EL spectrum from the device shows the main features expected from emission at the silicon band edge, including, at 1,190 nm, the phonon replica of the main peak at 1,130 nm. The room-temperature EL spectrum has the main peak at 1,160 nm with a full-width at half-maximum of 80 nm. No EL or photoluminescence (PL) is observed at any other wavelengths, even at low temperatures—a result that we again attributed to the close spatial confinement of carriers within regions of bulk silicon. The temperature dependence of the integrated EL intensity is shown in Fig. 4. In most systems, demonstrated for light emission in silicon[5,6,7] the EL quenches very strongly with increasing temperature, making practical room-temperature devices problematic. Here, it can be seen that the EL intensity actually increases as we go up in temperature. A similar behaviour has been observed but not explained in laser-recrystallized silicon[9]. The device is therefore, as required, most efficient at room temperature and above. Inset in Fig. 4 is a plot of the integrated PL intensity as a function of measurement tempera-

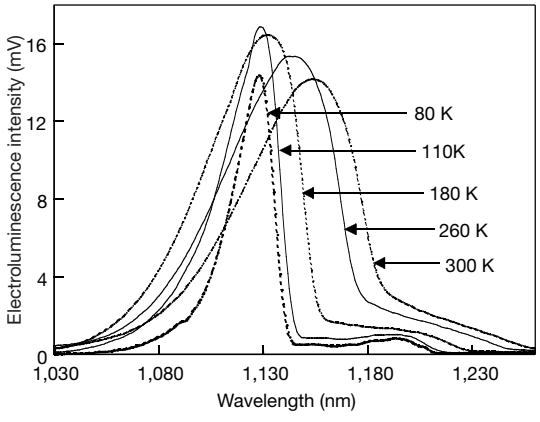

Figure 3 Spectra of the electroluminescence intensity against wavelength at various temperatures. The device was operated at a forward current of 50 mA for all temperatures.

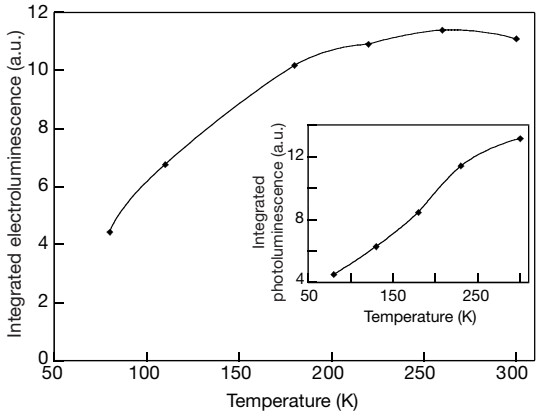

Figure 4 A plot of the integrated electroluminescence intensity as a function of measurement temperature. Inset, a plot of the integrated photoluminescence intensity as a function of temperature. The solid lines are provided as a guide to the eye. The photoluminescence was excited by the 488 nm line of an argon laser at a power of 150 mW.

© 2001 Macmillan Magazines Ltd

ture. The integrated PL also increases with temperature in the same manner as the EL, indicating that the temperature dependence is intrinsic to the recombination, rather than the injection mechanism. The strong temperature quenching of PL and EL in most semiconductors is primarily the result of the strong temperature dependence of the competing non-radiative routes—the band-to-band transition is relatively temperature-independent. In our case spatial localization of the radiative carrier population decouples it from any non-radiative recombination occurring elsewhere, thus eliminating the luminescence quenching. A full understanding of the form of the weak increase of the integrated intensity with temperature seen requires further investigation; it could be associated with increased scattering within the confined carrier populations and the increase in the effective density of band states with temperature. We have also carried out EL frequency-resolved measurements that give a device response time, at room temperature, of $18 \pm 2\,\mu s$. The PL and EL are both superlinear with excitation power and drive current respectively, meaning that the device improves further as we drive the device harder. In ref. 9 a similar dependence of the luminescence intensity is attributed, owing to a shift in emission wavelength, to sample heating. However, in our case, no such shift is observed.

The external quantum efficiency of our unpackaged planar device has been measured, based only on the light emitted just through the back window. At a 100 mA forward current the emitted light is 19.8 μW giving an external quantum efficiency of $(2.0 \pm 0.1) \times 10^{-4}$ at room temperature. We also obtain significant edge emission from the device, of a further 80 μW, but this is not included in our estimate of the quantum efficiency above. Taking it into account, our device has a quantum efficiency of 10^{-3}. The emitted power from the face of the device was measured by placing it immediately adjacent to a large-area calibrated power meter. The power meter is an Ophir Laser Star fitted with a PD300 IR head; the instrument is certificated and calibrated with standards traceable to the National Institute of Standards. Our front emitting devices have the same efficiencies as the back emitting devices. For comparison, commercially available GaAs infrared LEDs have typical external efficiencies of 10^{-2}. However, commercial packing of LEDs, in particular by minimizing the considerable internal reflection losses of the planar device and by collecting the edge emission, can improve the external efficiency by up to a factor of about 15. Our first, non-optimized devices are therefore already within a factor of 3 or so of the efficiencies achieved in conventional optimized LED devices.

We believe that the device demonstrated is the most likely candidate currently for implementing efficient light sources in silicon. Such a device would also form the basis for the development of an injection laser based on the same principles but with the incorporation of an optical cavity. The approach itself is not limited to silicon but could be applied to other materials, particularly other indirect materials and silicon alloys. For example, going from germanium to silicon to silicon carbide could produce devices, using the same approach, that could span the near-infrared region, including the 1.3 μm and 1.5 μm wavelength regions of the spectrum, important for optical fibre communications, and up to the ultraviolet region. □

Received 23 October 2000; accepted 29 January 2001.

1. European Commission *Technology Roadmap—Optoelectronic Interconnects for Integrated Circuits* (eds Forchel, A. & Malinverni, P.) (Office for Official Publications of the European Communities, Luxembourg, 1998).
2. Hirschman, K. D., Tysbekov, L., Duttagupta, S. P. & Fauchet, P. M. Silicon-based visible light-emitting devices integrated into microelectronic circuits. *Nature* **384,** 338–341 (1996).
3. Lu, Z. H., Lockwood, D. J. & Baribeau, J.-M. Quantum confinement and light emission in SiO_2/Si superlattices. *Nature* **378,** 258–260 (1995).
4. Komoda, T. *et al.* Visible photoluminescence at room temperature from microcrystalline silicon precipitates in SiO2 formed by ion implantation. *Nucl. Instrum. Methods B* **96,** 387–391 (1995).
5. Zheng, B. *et al.* Room-temperature sharp line electroluminescence at λ = 1.54 μm from an erbium-doped, silicon light-emitting diode. *Appl. Phys. Lett.* **64,** 2842–2844 (1994).
6. Vescan, L. & Stoica, T. Room-temperature SiGe light-emitting diodes. *J. Luminescence* **80,** 485–489 (1999).
7. Leong, D., Harry, M., Reeson, K. J. & Homewood, K. P. A silicon/iron disilicide light-emitting diode operating at a wavelength of 1.5 μm. *Nature* **387,** 686–688 (1997).
8. Tybeskov, L., Moore, K. L., Hall, D. G. & Fauchet, P. M. Intrinsic band-edge photoluminescence from silicon clusters at room temperature. *Phys. Rev. B* **54,** R8361–R8364 (1996).
9. Sveinbjörnsson, E. O. & Weber, J. Room temperature electroluminescence from dislocation rich silicon. *Appl. Phys. Lett.* **69,** 2686–2688 (1996).
10. Hirth, J. P. & Lothe, J. *Theory of Dislocations* 2nd edn, 63 (John Wiley & Sons, New York, 1982).

Correspondence and requests for materials should be addressed to K.P.H. (e-mail: k.homewood@eim.surrey.ac.uk).

Dating of the oldest continental sediments from the Himalayan foreland basin

Yani Najman*§, Malcolm Pringle†, Laurent Godin‡§ & Grahame Oliver¶

* *Fold and Fault Research Project, Department of Geology and Geophysics, University of Calgary, 2500 University Drive NW, Calgary, AB, Canada T2N 1N4*
† *Scottish Universities Environmental Research Centre, Scottish Enterprise Technology Park, Rankine Avenue, East Kilbride G75 0QF, UK*
‡ *Department of Earth Sciences, Oxford University, Parks Road, Oxford OX1 3PR, UK*
¶ *Crustal Geodynamics Group, School of Geography and Geosciences, Purdie Building, The University, St Andrews, Fife KY16 9ST, UK*

A detailed knowledge of Himalayan development is important for our wider understanding of several global processes, ranging from models of plateau uplift to changes in oceanic chemistry and climate[1–4]. Continental sediments 55 Myr old found in a foreland basin in Pakistan[5] are, by more than 20 Myr, the oldest deposits thought to have been eroded from the Himalayan metamorphic mountain belt. This constraint on when erosion began has influenced models of the timing and diachrony of the India–Eurasia collision[6–8], timing and mechanisms of exhumation[9,10] and uplift[11], as well as our general understanding of foreland basin dynamics[12]. But the depositional age of these basin sediments was based on biostratigraphy from four intercalated marl units[5]. Here we present dates of 257 detrital grains of white mica from this succession, using the ^{40}Ar–^{39}Ar method, and find that the largest concentration of ages are at 36–40 Myr. These dates are incompatible with the biostratigraphy unless the mineral ages have been reset, a possibility that we reject on the basis of a number of lines of evidence. A more detailed mapping of this formation suggests that the marl units are structurally intercalated with the continental sediments and accordingly that biostratigraphy cannot be used to date the clastic succession. The oldest continental foreland basin sediments containing metamorphic detritus eroded from the Himalaya orogeny therefore seem to be at least 15–20 Myr younger than previously believed, and models based on the older age must be re-evaluated.

The Balakot Formation, located in the Hazara–Kashmir Syntaxis of Northern Pakistan, is a continental foreland basin sedimentary sequence that contains detritus eroded from the India–Eurasia suture zone and the metamorphic rocks of the Himalaya[11]. The Balakot Formation overlies the Palaeocene shallow marine Patala Formation (Figs 1 and 2) and consists of a >8-km-thick fossil-free

§ Present addresses: Department of Geology & Geophysics, Edinburgh University, West Mains Road, Edinburgh EH9 3JW, UK (Y.N.); Department of Earth Sciences, Simon Fraser University, 8888 University Drive, Burnaby BC, V5A 1S6, Canada (L.G.).

© 2001 Macmillan Magazines Ltd

Acknowledgements

We acknowledge financial support of the Deutsche Forschungsgemeinschaft and of Roche Diagnostics. P. Göttig and R. Ramachandran helped with biochemical analyses. We thank G. Bourenkov and H. Bartunik, and G. Leonard for help with synchrotron data collection at DESY BW6 (Hamburg) and ESRF ID14-4 (Grenoble), respectively.

Competing interests statement

The authors declare that they have no competing financial interests.

Correspondence should be addressed to H.B. (e-mail: hbs@biochem.mpg.de). The coordinates of the tricorn protease have been deposited in Protein Data Bank under accession code 1K32.

addendum

An efficient room-temperature silicon-based light-emitting diode

Wai Lek Ng, M. A. Lourenço, R. M. Gwilliam, S. Ledain, G. Shao & K. P. Homewood

Nature **410,** 192–194 (2001).

Silicon light-emitting diodes (LED) show light emission at the bandgap energy of silicon with efficiencies approaching those of standard III–V emitters: 0.1% for planar devices (our Letter) and about 1% when total internal reflection is minimized by surface texturing[1]. We point out here an additional example of a silicon device also showing light emission at the bandgap[2]. The authors described devices made by the SACMOS-3 process and focus the bulk of the paper on visible emission under reverse bias. However, they also report briefly on a device operated under forward bias giving efficiencies of around 0.01%, although no explanation of the mechanism is given. It is now becoming clear that crystalline silicon, when appropriately engineered, is capable of supporting efficient light emission, opening up many significant applications. □

1. Green, M. A., Shao, J., Wang, A., Reece, P. J. & Gal, M. Efficient silicon light-emitting diodes. *Nature* **412,** 805–808 (2001).
2. Kramer, J. *et al.* Light-emitting devices in industrial CMOS technology. *Sensors Actuators* **A37–A38,** 527–533 (1993).

erratum

Warm tropical sea surface temperatures in the Late Cretaceous and Eocene epochs

Paul N. Pearson, Peter W. Ditchfield, Joyce Singano, Katherine G. Harcourt-Brown, Christopher J. Nicholas, Richard K. Olsson, Nicholas J. Shackleton & Mike A. Hall

Nature **413,** 481–487 (2001).

In this Article, the temperature scale in Figure 3i should have been the same as in Figure 3g. □

corrections

Self-assembled monolayer organic field-effect transistors

Jan Hendrik Schön, Hong Meng & Zhenan Bao

Nature **413,** 713–716 (2001).

The values of the transconductance in Table 1 and in the text (page 715, second paragraph) are incorrect. The values should be divided by ten. The data plotted in Figs 2 and 3 are correct and the conclusions are not affected. □

Ordered nanoporous arrays of carbon supporting high dispersions of platinum nanoparticles

Sang Hoon Joo, Seong Jae Choi, Ilwhan Oh, Juhyoun Kwak, Zheng Liu, Osamu Terasaki & Ryong Ryoo

Nature **412,** 169–172 (2001).

We inadvertently omitted to cite an earlier reference alongside ref. 8 (G. Che, B. Lakshmi, E. R. Fisher and C. R. Martin *Nature* **393,** 346–349; 1998), which was published in 1995 (and not 2000 as printed). Also, our suggestion that using the pores in a microporous material as templates could be a way in which to produce nanoscale materials has been discussed before (see, for example, C. R. Martin *Science* **266,** 1961–1966 (1994) and J. C. Hulteen & C. R. Martin *J. Mater. Chem.* **7,** 1075–1087 (1997)). □

The timing of the last deglaciation in North Atlantic climate records

Claire Waelbroeck, Jean-Claude Duplessy, Elisabeth Michel, Laurent Labeyrie, Didier Paillard & Josette Duprat

Nature **412,** 724–727 (2001).

We directly used the observed leads of sea surface temperature with respect to air temperature (dated in calendar years), whereas the air temperature calendar ages should have been converted into ^{14}C ages, with reservoir ages computed as the difference between marine and atmospheric ^{14}C ages. Taking this into consideration, apparent surface-water ages are 1,180 ± 630 to 1,880 ± 750 years at the end of the Heinrich 1 surge event (14,500 years BP) and 930 ± 250 to 1,050 ± 230 years at the end of the Younger Dryas cold episode. This does not change the discussion and conclusions. □

© 2001 Macmillan Magazines Ltd